10. Tamm, I. *et al.* Expression and prognostic significance of IAP-family genes in human cancers and myeloid leukemias. *Clin. Cancer Res.* **6,** 1796–1803 (2000).
11. Ambrosini, G., Adida, C. & Altieri, D. C. A novel anti-apoptosis gene, survivin, expressed in cancer and lymphoma. *Nature Med.* **3,** 917–217 (1997).
12. LaCasse, E. C., Baird, S., Korneluk, R. G. & MacKenzie, A. E. The inhibitors of apoptosis (IAPs) and their emerging role in cancer. *Oncogene* **17,** 3247–3259 (1998).
13. Sun, C. *et al.* NMR structure and mutagenesis of the inhibitor-of-apoptosis protein XIAP. *Nature* **401,** 818–822 (1999).
14. Sun, C. *et al.* NMR structure and mutagenesis of the third BIR domain of the inhibitor of apoptosis protein XIAP. *J. Biol. Chem.* **275,** 33777–33781 (1998).
15. Verdecia, M. A. *et al.* Structure of the human anti-apoptotic protein survivin reveals a dimeric arrangement. *Nature Struct. Biol.* **7,** 602–608 (2000).
16. Muchmore, S. W. *et al.* Crystal structure and mutagenic analysis of the inhibitor-of-apoptosis protein survivin. *Mol. Cell* **6,** 173–182 (2000).
17. Chantalat, L. *et al.* Crystal structure of human survivin reveals a bow-tie-shaped dimer with two unusual α-helical extensions. *Mol. Cell* **6,** 183–189 (2000).
18. Kleywegt, G. J. & Jones, T. A. in *From First Map to Final Model* (eds Bailey, S., Hubbard, R. & Waller, D.) 59–66 (Daresbury Laboratory, Daresbury, UK, 1994).
19. Vucic, D., Kaiser, W. J. & Miller, L. K. Inhibitor of apoptosis proteins physically interact with and block apoptosis induced by *Drosophila* proteins Hid and Grim. *Mol. Cell Biol.* **18,** 3300–3309 (1998).
20. Cutforth, T. & Gaul, U. A methionine aminopeptidase and putative regulator of translation initiation is required for cell growth and patterning in *Drosophila*. *Mech. Dev.* **82,** 23–28 (1999).
21. Clore, G. M. & Gronenborn, A. M. Multidimensional heteronuclear magnetic resonance of proteins. *Methods Enzymol.* **239,** 349–363 (1994).
22. Cornilescu, G., Delaglio, F. & Bax, A. Protein backbone angle restraints from searching a database for chemical shift and sequence homology. *J. Biomol. NMR* **13,** 289–302 (1999).
23. Stein E. G., Rice, L. M. & Brünger, A. T. Torsion-angle molecular dynamics as a new efficient tool for NMR structure calculation. *J. Magn. Reson. B* **124,** 154–164 (1997).
24. Nilges, M., Gronenborn, A. M., Brünger, A. T. & Clore, G. M. Determination of three-dimensional structures of proteins by simulated annealing with interproton distance restraints. Application to crambin, potato carboxypeptidase inhibitor and barley serine proteinase inhibitor 2. *Protein Eng.* **2,** 27–38 (1988).
25. Nilges, M., Macias, M. J., O'Donoghue, S. I. & Oschkinat, H. Automated NOESY interpretation with ambiguous distance restraints: The refined NMR solution structure of the pleckstrin homology domain from β-spectrin. *J. Mol. Biol.* **269,** 408–422 (1997).
26. Laskowski, R. A., Rullmann, J. A., MacArthur, M. W., Kaptein, R. & Thornton, J. M. AQUA and PROCHECK-NMR: Programs for checking the quality of protein structures solved by NMR. *J. Biomol. NMR* **8,** 477–486 (1996).
27. Carson, M. J. Ribbon models of macromolecules. *J. Mol. Graphics* **5,** 103–106 (1987).

Acknowledgements

We thank L. Barrett and P. Richardson for help in the synthesis of some of the peptides, L. Miesbauer for the mass spectrometry data, and J. Noel and co-workers for the coordinates of human survivin.

Correspondence and requests for materials should be addressed to S.W.F. (e-mail: Stephen.Fesik@abbott.com). Coordinates for the NMR structure of the XIAP BIR3/Smac peptide complex have been deposited in the Brookhaven Protein Data Bank under accession code 1G3F.

Structural basis of IAP recognition by Smac/DIABLO

Geng Wu*†, Jijie Chai*†, Tomeka L. Suber‡, Jia-Wei Wu*, Chunying Du§, Xiaodong Wang§ & Yigong Shi*

** Department of Molecular Biology, Princeton University, Lewis Thomas Laboratory, Washington Road, Princeton, New Jersey 08544, USA*
‡ 310 Aycock Dorm, University of North Carolina at Chapel Hill, Chapel Hill, North Carolina 27514, USA
§ Department of Biochemistry and Howard Hughes Medical Institute, University of Texas Southwestern Medical Center, Dallas, Texas 75235, USA
† These authors contributed equally to this work

Apoptosis is an essential process in the development and homeostasis of all metazoans[1–4]. The inhibitor-of-apoptosis (IAP) proteins suppress cell death by inhibiting the activity of caspases; this inhibition is performed by the zinc-binding BIR domains[5,6] of the IAP proteins. The mitochondrial protein Smac/DIABLO promotes apoptosis by eliminating the inhibitory effect of IAPs through physical interactions[7–9]. Amino-terminal sequences in Smac/DIABLO are required for this function, as mutation of the very first amino acid leads to loss of interaction with IAPs and concomitant loss of Smac/DIABLO function[9]. Here we report the high-resolution crystal structure of Smac/DIABLO complexed with the third BIR domain (BIR3) of XIAP. Our results show that the N-terminal four residues (Ala-Val-Pro-Ile) in Smac/DIABLO recognize a surface groove on BIR3, with the first residue Ala binding a hydrophobic pocket and making five hydrogen bonds to neighbouring residues on BIR3. These observations provide a structural explanation for the roles of the Smac N terminus as well as the conserved N-terminal sequences in the *Drosophila* proteins Hid/Grim/Reaper. In conjunction with other observations, our results reveal how Smac may relieve IAP inhibition of caspase-9 activity. In addition to explaining a number of biological observations, our structural analysis identifies potential targets for drug screening.

All members of the IAP family contain at least one BIR (baculoviral IAP repeat) motif and many contain three. Recent experiments indicate that different BIR domains may exhibit distinct functions. The second BIR domain (BIR2) of XIAP is a potent inhibitor for caspase-3, whereas the third BIR domain of XIAP (XIAP-BIR3) primarily targets the active caspase-9[10–13]. Smac is synthesized as a precursor molecule of 239 amino acids; the N-terminal 55 residues serve as the mitochondria targeting sequence that is removed after import[7]. The wild-type Smac protein (residues 1–184) forms a dimer in solution and interacts with both the BIR2 and BIR3 domains of XIAP[9]. Point mutations at the dimeric interface, such as Phe33→Asp, completely inactivate dimer formation[9]. Such monomeric mutants can no longer interact with XIAP-BIR2, but they retain binding to the BIR3 domain[9]. A missense mutation of the N-terminal Ala residue to Met (Ala1→Met) in wild-type Smac abolishes binding to both the BIR2 and BIR3 domains of XIAP and results in complete loss of Smac function[9]. In support of its critical role, a short 7-residue peptide derived from the Smac N-terminus was able to promote the activation of procaspase-3[9], raising the possibility of using small peptides or peptide mimics to treat cancer cells.

To provide a structural basis for IAP recognition by Smac, we crystallized the wild-type Smac in complex with either the BIR2 or the BIR3 domain of XIAP. But these crystals did not diffract X-rays well. To facilitate crystallization, we reconstituted binary complexes using a monomeric Smac protein (with the missense mutation Phe33→Asp). Crystals of this mutant Smac with XIAP-BIR3 (residues 238–358) were obtained in two different conditions, neither of which disrupted interactions between Smac and XIAP-BIR3 in solution. We have determined these two crystal structures of the binary complex at 2.0 and 2.6 Å (see Methods and Supplementary Information). There are two identical complexes in each asymmetric unit in each of the two crystal forms. Although the packing interactions are different, two sets of conserved interaction interfaces between Smac and XIAP-BIR3 are present in these two crystal forms, with 0.95 Å root-mean-square-deviation (r.m.s.d.) for all aligned Cα atoms (Fig. 1a). Because of these conserved features, we limit our discussions to the 2.0 Å structure (Fig. 1b).

In the complex, the Smac protomer is an elongated three-helix bundle (Fig. 1), very similar to the structure of Smac by itself (0.7 Å r.m.s.d. for aligned Cα atoms)[9]. XIAP-BIR3 consists of six α-helices, a three-stranded β-sheet, and a zinc atom chelated by three Cys and one His residues (Cys 300, Cys 303, His 320 and Cys 327) (Fig. 1). The XIAP-BIR3 structure closely resemble those of other BIR domains[14], with approximately 1.22 and 1.38 Å r.m.s.d. to the aligned Cα atoms of survivin[15,16] and cIAP1-BIR2[12], respectively. In the crystals, Smac recognizes XIAP-BIR3 with two interfaces. First, the N-terminal four residues in Smac, Ala1-Val2-Pro3-Ile4, bind a surface groove on BIR3 formed by the strand β3, the helix α3 and the intervening loop. Two of these four residues, Val2 and Pro3, form a short anti-parallel β-strand with the three-stranded β-sheet

of BIR3 (Figs 1a and 2a). Second, the helices H2 and H3 in Smac contact the BIR3 residues surrounding the helix α1 (Fig. 1a). The N-terminal residues and the H2–H3 helices in Smac that contact the same BIR3 domain are from two different Smac protomers (Fig. 1b). The N-terminus of one Smac protomer extends out and recognizes a BIR3 domain that interacts with another Smac protomer through the second interface (Fig. 1b). This arrangement is in agreement with our structure-based prediction[9].

The N-terminal four residues of Smac pack into a surface groove on XIAP-BIR3, resulting in the burial of 892 Å^2 exposed surface area (Fig. 2b). The recognition specificity is achieved through a combination of hydrogen-bond interactions and van der Waals contacts (Fig. 2a). A total of eight inter- and three intra-molecular hydrogen bonds support the binding of the Smac tetrapeptide (Ala1-Val2-Pro3-Ile4) in the surface groove on BIR3. Three intermolecular contacts between the backbone groups of Val2/Ile4 in Smac and Gly306/Thr308 in BIR3 allow the formation of a four-stranded antiparallel β-sheet (Fig. 2c). The remaining hydrogen bonds constitute an intricate network surrounding the N-terminal residue Ala1. At the centre of the network, the amino group of Ala 1 donates three hydrogen bonds to Glu 314 and Gln 319 whereas its carbonyl group makes two additional contacts to Gln 319 and Trp 323 (Fig. 2c). At the periphery of the network, three intra-molecular contacts further buttress the interactions (Fig. 2c).

In addition to the hydrogen-bond network, van der Waals contacts also appear to be important in stabilizing the interactions between the Smac tetrapeptide and the BIR3 surface groove. The methyl group of Ala 1 fits tightly in a hydrophobic pocket formed by the side chains of Leu 307, Trp 310 and Gln 319 (Fig. 2c). Stereochemical parameters indicate that replacement of Ala 1 by any other residue except Gly will cause steric hindrance in this pocket, probably weakening binding and abolishing hydrogen bonds by the amino and carbonyl groups of Ala 1. This observation explains the finding that the mutation Ala1→Met in Smac completely eliminated interaction with the BIR domains[9]. The absolute requirement for Ala as the N-terminal residue is also consistent with the observation that the mutant Smac-del4 retained weak interaction with the BIR domains[9], as removal of the first four residues in Smac leaves Ala 5 as the N-terminal residue. We predict that Ala 1 cannot be replaced by Gly because of the associated entropic penalty and loss of van der Waals interactions, although we have not tested this prediction.

The bulky, flat aromatic side chain of Trp 323 is important in forming the surface groove on BIR3 (Fig. 2c). Both Val 2 and Pro 3

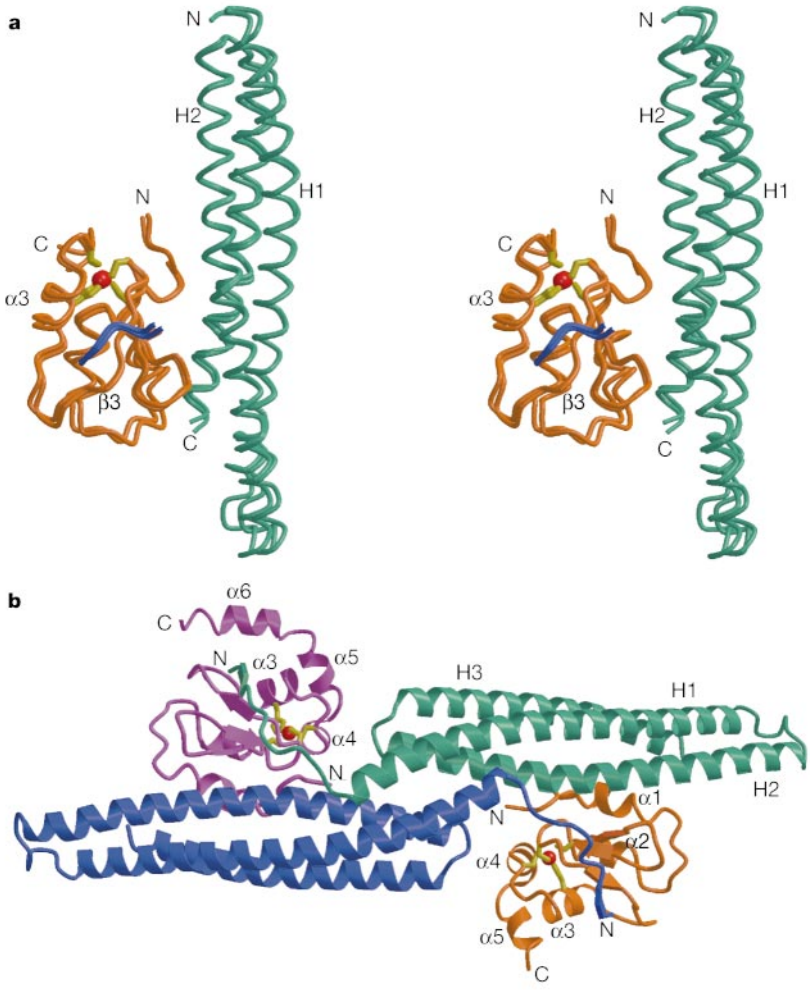

Figure 1 Schematic representation of the Smac(Phe33→Asp)/XIAP-BIR3 structures. **a,** Stereo view of superimposition of the two structures from two different crystal forms. Smac and XIAP-BIR3 are coloured green and orange, respectively. The bound Smac N-terminal peptide is shown in blue. The zinc atom is highlighted in red whereas its chelating residues are shown in yellow. **b,** Schematic representation of the complete structure in one asymmetric unit. Two Smac protomers are coloured green and blue, respectively. Two BIR3 domains are shown in orange and pink, respectively. Some secondary structural elements are labelled. In the crystals, each Smac protomer uses its extended N terminus to bind a BIR3 domain whereas it interacts with a second BIR3 domain with a different interface. All figures were prepared with MOLSCRIPT[26] and GRASP[27].

maintain multiple van der Waals interactions with Trp 323, while Pro 3 makes additional contact to Tyr 324 (Fig. 2c). In addition, the side chain of Ile 4 interacts with Leu 292, Gly 306, and the aliphatic side chains of Lys 297 and Lys 299. Of these residues, Gly 306 appears to be particularly important, because the absence of a side chain at this position makes these interactions possible (Fig. 2c). Although Ala 5 and Gln 6 in Smac are ordered in the crystals, they do not make important interactions to the BIR3 domain; nor are they involved in binding the surface groove.

Among the N-terminal four residues, Ala 1 makes the largest contribution to the specific recognition of XIAP. The next three residues, Val 2, Pro 3 and Ile 4, are all hydrophobic, and they interact with the hydrophobic residues lining the BIR3 surface groove. These residues also contribute to the appropriate positioning of Ala 1 in the pocket (Fig. 2c); however, their identity does not appear to be as critical as that of the N-terminal Ala 1.

Our structural analysis has identified several residues in XIAP-BIR3 that mediate crucial interactions with Smac. To confirm these structural observations, we created nine missense mutations on BIR3 and examined their interaction with Smac using purified recombinant proteins. Consistent with their important roles in binding the Smac N-terminus, point mutation to Ala or Arg for any of the three residues Glu 314, Gln 319 and Trp 323 significantly reduced or abolished interaction with the wild-type Smac protein, presumably because of the disruption of binding to the Smac tetrapeptide (data not shown). In contrast, three control mutations outside the peptide-binding surface, Glu282→Ala, Glu282→Arg and Arg286→Glu, had no detectable effect on the interaction between XIAP-BIR3 and Smac (data not shown).

In *Drosophila*, three proteins, Hid, Grim and Reaper, appear to be the functional homologues of the mammalian Smac[9]. These three proteins appear to act upstream of the *Drosophila* IAP, DIAP1, and physically interact with DIAP1 to relieve its inhibitory effect on caspase activation[17,18]. Although previous sequence alignment between Smac and the *Drosophila* proteins failed to reveal significant homology, our results showing a Smac tetrapeptide binding to XIAP motivated us to re-examine the N-terminal sequences of Hid/Grim/Reaper. This analysis revealed notable similarity in the N termini of these proteins (Fig. 2d). All three *Drosophila* proteins begin with Ala; both Reaper and Hid have Val in the second position whereas Grim replaces Val with a conserved Ile. This sequence conservation strongly suggests that the *Drosophila* proteins Hid/Grim/Reaper may interact with DIAP1 in a similar fashion, and that the N-terminal sequences from Hid/Grim/Reaper may recognize the same surface groove. This analysis also predicts that (1) the initiating Met residue in Hid/Grim/Reaper is removed by a methionyl peptidase in *Drosophila* as is the case in *Escherichia coli*[9,19], and (2) other pro-apoptotic proteins bearing N-terminal homology to the Ala-Val-Pro-Ile sequence may remain to be discovered.

In addition to the peptide-binding groove, we also observed a second interaction interface between Smac and the BIR3 domain of XIAP (Fig. 2e). Residues around the helix α1 in BIR3 pack against the middle portion of helices H2 and H3 in Smac. This interface consists of seven hydrogen bonds and two patches of van der Waals interactions, with over 2,000 Å^2 of buried surface area (Fig. 2e). The hydrogen bonds cluster in a small area, where Glu 99 and Thr 100 in Smac make six contacts to Asn 259, Ser 261 and Arg 258 (Fig. 2e). In addition, Arg 85 on helix H2 donates one hydrogen bond to the side chain of Thr 274 (Fig. 2e). Although van der Waals interactions are scattered throughout the large interface (Fig. 2e), there are two prominent patches. First, Phe 270 on helix α1 of XIAP-BIR3 extends out into a hydrophobic pocket formed by the side chains of Met 88, Leu 153, Ala 154, Gln 157 and Glu 150 (Fig. 2e). Second, Leu 96 on helix H2 makes multiple contacts to the side chains of Met 262 and

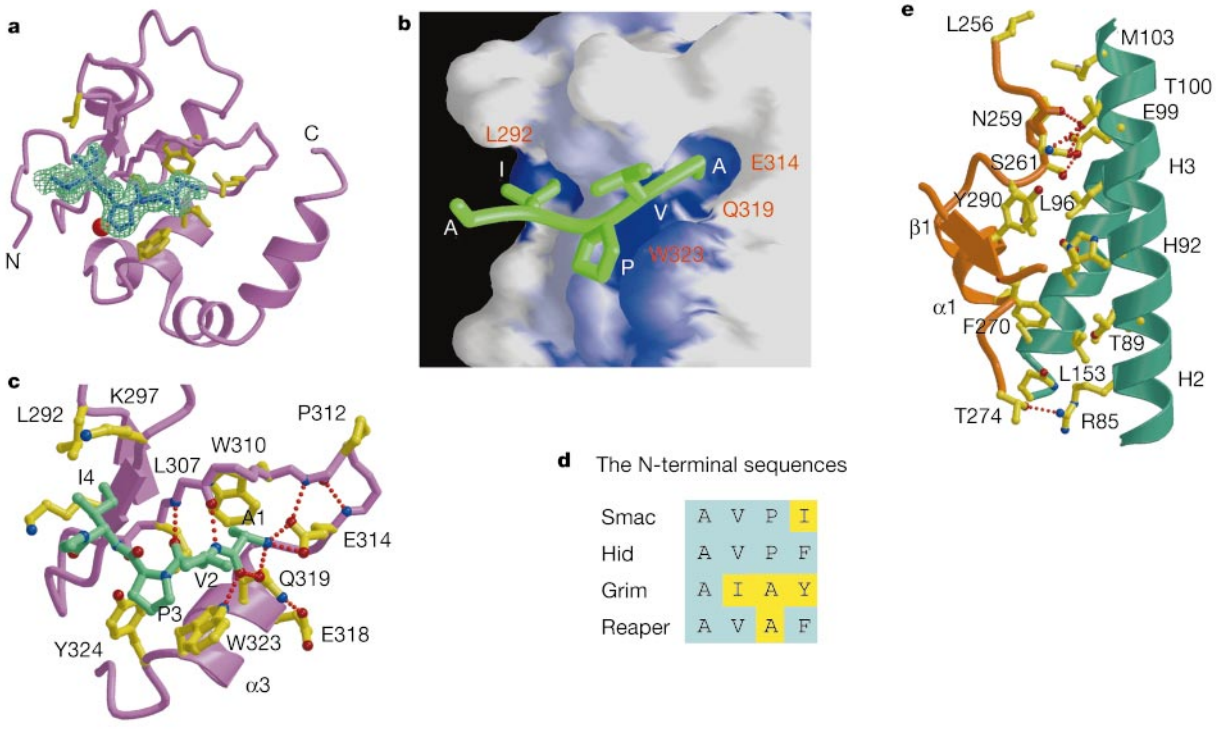

Figure 2 Binding interface between Smac and XIAP-BIR3. **a,** Overall view of the interaction between Smac N-terminal residues and XIAP-BIR3. Smac is coloured blue and the interface residues from BIR3 are highlighted in yellow. The zinc atom is shown in red. The F_o–F_c electron density (omit map), shown in green, was contoured at 2.5σ and calculated with simulated annealing using XPLOR[24] with the omission of the Smac N-terminal seven residues. **b,** Close-up view of the binding groove on BIR3 for the Smac N terminus. The blue and white colours represent the most and least hydrophobic surfaces, respectively. The N-terminal five residues of Smac are shown in green. **c,** Close-up view of the interaction between the Smac N terminus and the surface groove on BIR3. Smac and BIR3 are coloured green and pink, respectively. Hydrogen bonds are represented by red dashed lines. Oxygen and nitrogen atoms are shown as red and blue balls, respectively. **d,** Alignment of the N-terminal four amino acids of Smac with those from the *Drosophila* proteins Hid, Grim and Reaper. **e,** Close-up view of a second interface between Smac and XIAP-BIR3. Smac and BIR3 are coloured green and orange, respectively.

Tyr 290 (Fig. 2e). Although the buried surface area is relatively large for this interaction interface, shape complementarity between Smac and BIR3 is not optimal. Compared to the binding of the Smac N-terminal tetrapeptide to the surface groove on BIR3, this interface is likely to play a minor role. This analysis is consistent with the observation that N-terminal deletion mutants of Smac failed to bind XIAP-BIR3[9].

Wild-type Smac interacts with the BIR2 and BIR3 of XIAP but does not bind the BIR1 domain[9]. To explain this observation, we compared the primary sequences of the BIR domains from XIAP and cIAP-1. Among the many residues that line the BIR3 surface groove, five appear to be mediating critical contacts with Smac. Leu 307 and Trp 310 are involved in pocket formation for the side chain of Ala 1 of Smac; Glu 314 hydrogen-bonds to Ala 1; Trp 323 interacts with Val 2 and Pro 3 and hydrogen-bonds to Ala 1; Gly 306 allows docking of Ile 4. Among these five residues, Trp 310 is invariant; Leu 307 and Glu 314 are highly conserved among all BIR domains. The replacement of Gly 306 by other residues in BIR2 and BIR1 probably disrupts tight packing of Ile 4 of Smac against residues in the BIR domain. More importantly, Trp 323 is replaced by His in the BIR2 domain and Val/Leu in the BIR1 domain, which may alter the lining of the surface groove. The replacement of Trp 323 by His in BIR2 is likely to be less deleterious than its replacement by Val/Leu; this is because His may retain the hydrogen bond contact to the carbonyl group of Ala 1 in Smac (Fig. 2c). These analyses are consistent with the observations that wild-type Smac does not interact with BIR1 and that monomeric Smac mutants fail to bind BIR2[9].

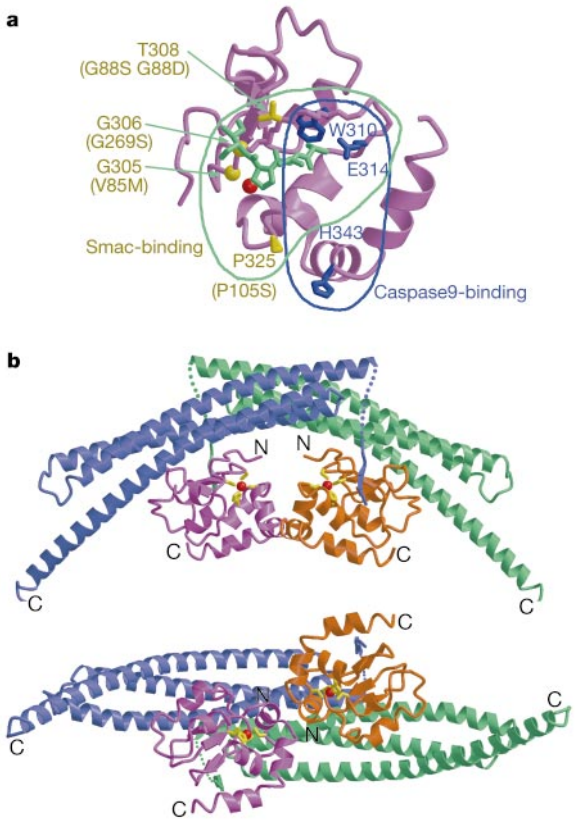

Figure 3 Proposed mechanism for the relief of XIAP inhibition of caspase-9 by Smac. **a,** The surface on XIAP-BIR3 that binds to caspase-9 overlaps with the Smac-binding groove. XIAP-BIR3 is primarily responsible for inhibiting caspase-9[10,13]. Mutation of the three residues, W310, E314 and H343 (coloured blue), prevents caspase-9 inhibition by XIAP-BIR3[13]. Four residues, T308, G305, G306 and P325, are shown in yellow. Mutation of the corresponding residues in the *Drosophila* protein DIAP1 (shown in parentheses) leads to a gain-of-function phenotype[18,20]. **b**, Proposed structure of a wild-type Smac/XIAP-BIR3 complex (see text). Two perpendicular views are shown.

The BIR3 domain of XIAP is primarily responsible for the inhibition of caspase-9 activity[10,13]. How does Smac relieve this inhibition? Both published observations and current analysis suggest a model of mutual exclusion of caspase-9 and Smac for binding to the BIR3 domain. Three mutations in XIAP-BIR3, Glu314→Ser, Trp310→Ala and His343→Ala, abolish inhibition of caspase-9 activity[13], suggesting that the affected residues may directly contact caspase-9 and inhibit its activity. Indeed, the three affected residues are close to each other and two of them are directly involved in binding Smac tetrapeptide (Fig. 3a). In the structure, Trp 310 forms an important part of the pocket that accommodates Ala 1 in Smac, suggesting that binding by the Smac N terminus may evict a binding moiety of caspase-9 from the pocket. In addition, the amino group of Ala1 in Smac makes a pair of charge-stabilized hydrogen bonds to the side chain of Glu 314 in XIAP, probably competing with the interaction between Glu 314 and caspase-9. His343→Ala affects a residue that abuts the peptide-binding pocket, further supporting the mutual exclusion model (Fig. 3a).

Our structural analysis also provides a plausible explanation for gain-of-function (GOF) mutations in DIAP1. All five reported GOF mutations[18,20] appear to disrupt the peptide-binding groove and impair binding by the *Drosophila* proteins Hid/Grim/Reaper (Fig. 3a). For example, Gly269→Ser affects a residue that corresponds to G306 in XIAP-BIR3; Val85→Met and Gly88→Asp (or Gly88→Ser) affect residues that correspond to Gly 305 and Thr 308 in XIAP, respectively. These residues are either in the groove (Gly 306 and Thr 308) or in the vicinity of the groove (Gly 305). The fifth GOF mutation, Pro105→Ser, affects a corresponding residue (Pro 325) in XIAP that makes a sharp turn and allows Trp 323 to line the groove. We suggest that these five mutations impair binding of DIAP-1 to Hid/Grim/Reaper without significantly affecting binding to *Drosophila* caspases (Fig. 3a).

Although a Smac monomeric mutant (Phe33→Asp) was used for crystallization, there are two complexes in each asymmetric unit in the crystals (Fig. 1b). The two Smac protomers pack against each other using part of the wild-type dimeric interface (Fig. 1b). Docking the XIAP-BIR3 domain onto the wild-type Smac dimer structure using the BIR3:Smac interface observed here places the BIR3 domain underneath the arch-shaped Smac molecule (Fig. 3b). This arrangement also places two BIR3 domains next to each other (Fig. 3b). This model for the complex between wild-type Smac and BIR3 is consistent with available biochemical data. For example, XIAP-BIR2 does not interact with the monomeric mutants of Smac, suggesting that BIR2:BIR2 interactions may be required for stable binding of BIR2 to the wild-type dimeric Smac[9].

Our high-resolution crystal structure of a complex between Smac and the BIR3 domain of XIAP reveals a peptide-binding groove on the surface of BIR3 that is important in IAP function. This peptide-binding groove is lined with both hydrophobic and negatively charged residues, and appears to be a promising drug target. Future experiments need to be directed at identification and optimization of a high-affinity drug that is capable of promoting apoptosis in cancer cells. □

Methods

Site-directed mutagenesis and protein preparation

Point mutations were generated by PCR, and the identities of individual clones were verified by sequencing. Recombinant XIAP-BIR3 (residues 238–358) were overexpressed as GST-fusion proteins using pGEX-2T (Pharmacia). The mutant Smac protein (Phe33Asp, residues 1–162) was overexpressed in *E. coli* strain BL21(DE3) using a pET-3d vector (Novagen). Selenomethionyl Smac (Phe33Asp) was expressed in *E. coli* B834(DE3) (Novagen) in M9 minimal medium supplemented with 50 mg l^{-1} selenomethionine. Protein purification was performed as described[9]. The concentration of the final complex was approximately 15 mg ml^{-1}. For interaction assays, both wild-type and mutant Smac were overexpressed in *E. coli* strain BL21(DE3) as C-terminally 9-Histidine-tagged proteins using a pET-15b vector (Novagen).

In vitro interaction assay

Interaction between Smac and XIAP-BIR3 was examined by GST-mediated pull-down assays. Approximately 0.4 mg of a wild-type or mutant BIR3 fragment was bound to 200 μl of glutathione resin as a GST-fusion protein and incubated with 0.5 mg of wild-type or mutant Smac at room temperature. After extensive washing with an assay buffer containing 25 mM Tris, pH 8.0, 150 mM NaCl, and 2 mM dithiothreitol (DTT), the complex was eluted with 5 mM reduced glutathione and visualized by SDS-polyacrylamide gel electrophoresis (SDS-PAGE) with Coomassie staining.

Crystallization and data collection

Crystals were grown by the hanging-drop vapour-diffusion method by mixing the Smac/XIAP-BIR3 complex (15 mg ml^{-1}) with an equal volume of reservoir solution. At 4 °C, the reservoir contained 100 mM MES buffer, pH 6.5, 12% isopropanol (v/v), 200 mM sodium citrate, and 10 mM DTT. At 23 °C, the reservoir contained 100 mM citrate buffer, pH 5.5, 5% PEG 4000 and 10% isopropanol. Crystals appeared after 1–4 days and reached a maximum size over a period of 1–3 weeks. Both crystals are in the triclinic space group P1 and contain two complexes in each unit cell. However, the unit cell dimensions are significantly different. Crystals grown at 4 °C have a = 47.0 Å, b = 54.6 Å, c = 74.2 Å, α = 93.0°, β = 101.1°, and γ = 94.9°; crystals grown at 23 °C have a = 48.1 Å, b = 52.9 Å, c = 67.1 Å, α = 100.0°, β = 104.1°, and γ = 94.0.° Diffraction data were primarily collected using an R-AXIS-IV imaging plate detector mounted on a Rigaku 200HB generator. Derivatives were obtained by soaking crystals in reservoir buffer containing 20% glycerol (v/v) and heavy atoms. The concentration and soaking time for mercury thimerosal were 1 mM and 20 hours, respectively. To collect data at −170 °C, crystals were equilibrated in a cryoprotectant buffer containing reservoir buffer plus 20% glycerol (v/v) and were flash frozen in a cold nitrogen stream. The high-resolution native data were collected at the NSLS beamline X4A.

Structure determination

We focused on the crystals grown at 4 °C first, because of the availability of a high-quality selenomethionine derivative. The first six selenium positions were determined using SOLVE[21] and further refined using MLPHARE[22]. The positions of the other four selenium atoms and mercury thimerosal were identified using difference Fourier methods. Initial MIR phases calculated with the program MLPHARE[22] had a mean figure of merit of 0.404 to 3.0 Å resolution, and were improved with solvent flattening and histogram matching using the program DM[22]. The electron density for the Smac N-terminal four residues was very clear in the experimental map. A model was built into MIR electron density with the program O[23] and refined at 2.6 Å resolution by simulated annealing using the program XPLOR[24]. Non-crystallography symmetry (NCS) constraints were applied to all refinement cycles except the last one. The two refined complexes (R factor 24% and free R 28.5%) are nearly identical to one another, and contain Smac residues 1–6 and 13–157, XIAP residues 251–343, and 58 ordered water molecules. Residues 7–12 and 158–162 in Smac and the terminal residues in XIAP (238–250 and 344–358) have no electron density in the maps, and we presume that these regions are disordered in the crystals. After completion of the refinement for the crystals grown at 4 °C, the atomic coordinates of BIR3 and Smac were used individually to obtain molecular replacement solutions for the crystals grown at 23 °C, using AMoRe[25]. The solutions were combined in O[23]. Rigid body refinement by XPLOR[24] confirmed the correctness of the solutions. This model was further refined at 2.0 Å resolution by simulated annealing using the program XPLOR[24], followed by model building in O[23]. NCS was helpful for the initial cycles of refinement. The final refined model, with an R factor of 22.7% and free R of 26.8%, contains two complexes. One complex contains Smac 1–157 and XIAP 256–357, and the other complex contains Smac 1–157 and XIAP 256–343. Except for the C-terminal 14 residues of XIAP in the first complex, which is disordered in the second one, the structures of these two complexes are identical to one another.

Received 18 September; accepted 9 November 2000.

1. Steller, H. Mechanisms and genes of cellular suicide. *Science* **267,** 1445–1449 (1995).
2. Jacobson, M. D., Weil, M. & Raff, M. C. Programmed cell death in animal development. *Cell* **88,** 347–354 (1997).
3. Hengartner, M. O. Programmed cell death in invertebrates. *Curr. Opin. Genet. Dev.* **6,** 34–38 (1996).
4. Horvitz, H. R. Genetic control of programmed cell death in the nematode *Caenorhabditis elegans*. *Cancer Res.* **59,** 1701–1706 (1999).
5. Deveraux, Q. L. & Reed, J. C. IAP family proteins—suppressors of apoptosis. *Genes Dev.* **13,** 239–252 (1999).
6. Miller, L. K. An exegesis of IAPs: salvation and surprises from BIR motifs. *Trends Cell Biol.* **9,** 323–328 (1999).
7. Du, C., Fang, M., Li, Y. & Wang, X. Smac, a mitochondrial protein that promotes cytochrome c-dependent caspase activation during apoptosis. *Cell* **102,** 33–42 (2000).
8. Verhagen, A. M. *et al.* Identification of DIABLO, a mammalian protein that promotes apoptosis by binding to and antagonizing IAP proteins. *Cell* **102,** 43–53 (2000).
9. Chai, J. *et al.* Structural and biochemical basis of apoptotic activation by Smac/DIABLO. *Nature* **406,** 855–862 (2000).
10. Deveraux, Q. L. *et al.* Cleavage of human inhibitor of apoptosis protein XIAP results in fragments with distinct specificities for caspases. *EMBO J.* **18,** 5242–5251 (1999).
11. Takahashi, R. *et al.* A single BIR domain of XIAP sufficient for inhibiting caspases. *J. Biol. Chem.* **273,** 7787–7790 (1998).
12. Sun, C. *et al.* NMR structure and mutagenesis of the inhibitor-of-apoptosis protein XIAP. *Nature* **401,** 818–822 (1999).
13. Sun, C. *et al.* NMR structure and mutagenesis of the third BIR domain of the inhibitor of apoptosis protein XIAP. *J. Biol. Chem* **275,** 33777–33781 (2000).
14. Shi, Y. Survivin structure: crystal unclear. *Nature Struct. Biol.* **7,** 620–623 (2000).
15. Verdecia, M. A. *et al.* Structure of the human anti-apoptotic protein survivin reveals a dimeric arrangement. *Nature Struct. Biol.* **7,** 602–608 (2000).
16. Chantalat, L. *et al.* Crystal structure of human survivin reveals a bow-tie-shaped dimer with two unusual alpha helical extensions. *Mol. Cell* **6,** 183–189 (2000).
17. Wang, S., Hawkins, C., Yoo, S., Muller, H.-A. & Hay, B. The *Drosophila* caspase inhibitor DIAP1 is essential for cell survival and is negatively regulated by HID. *Cell* **98,** 453–463 (1999).
18. Goyal, L., McCall, K., Agapite, J., Hartwieg, E. & Steller, H. Induction of apoptosis by *Drosophila* reaper, hid and grim through inhibition of IAP function. *EMBO J.* **19,** 589–597 (2000).
19. Hirel, P.-H., Schmitter, J.-M., Dessen, P., Fayat, G. & Blanquet, S. Extent of N-terminal methionine excision from *Escherichia coli* proteins is governed by the side-chain length of the penultimate amino acid. *Proc. Natl Acad. Sci. USA* **86,** 8247–8251 (1989).
20. Lisi, S., Mazzon, I. & White, K. Diverse domains of THREAD/DIAP1 are required to inhibit apoptosis induced by REAPER and HID in *Drosophila*. *Genetics* **154,** 669–678 (2000).
21. Terwilliger, T. C. & Berendzen, J. Correlated phasing of multiple isomorphous replacement data. *Acta Crystallogr. D* **52,** 749–757 (1996).
22. Collaborative Computational Project. The CCP4 suite: programs for protein crystallography. *Acta Crystallogr. D.* **50,** 760–763 (1994).
23. Jones, T. A., Zou, J.-Y., Cowan, S. W. & Kjeldgaard, M. Improved methods for building protein models in electron density maps and the location of errors in these models. *Acta Crystallogr. A* **47,** 110–119 (1991).
24. Brunger, A. T. *X-PLOR, a System for Crystallography and NMR* (Yale Univ. Press, New Haven, Connecticut, 1991).
25. Navaza, J. AMoRe: an automated package for molecular replacement. *Acta Crystallogr. A* **50,** 157–163 (1994).
26. Klaulis, P. J. Molscript: a program to produce both detailed and schematic plots of protein structures. *J. Appl. Crystallogr.* **24,** 946–950 (1991).
27. Nicholls, A., Sharp, K. A. & Honig, B. Protein folding and association: insights from the interfacial and thermodynamic properties of hydrocarbons. *Proteins: Struct. Funct. Genet.* **11,** 281–296 (1991).

Supplementary information is available on *Nature*'s World-Wide Web site (http://www.nature.com) or as paper copy from the London editorial office of *Nature*.

Acknowledgements

We thank C. Ogata for help at the NSLS-X4A beamline; F. Hughson for critically reading the manuscript; S. Kyin for peptide sequencing, DNA synthesis and mass spectroscopy; and N. Hunt for secretarial assistance. This research is supported by start-up funds from Princeton University (Y.S.) and the Howard Hughes Medical Institute (X.W.). Y.S. is a Searle Scholar and a Rita Allen Scholar.

Correspondence and requests for materials should be addressed to Y.S. (e-mail: yshi@molbio.princeton.edu). Atomic coordinates for the Smac/BIR3 complex have been deposited at the Protein Data Bank with accession number 1G73.

correction

Digital selection and analogue amplification coexist in a cortex-inspired silicon circuit

Richard H. R. Hahnloser, Rahul Sarpeshkar, Misha A. Mahowald, Rodney J. Douglas & H. Sebastian Seung

Nature **405,** 947–951 (2000).

There were two errors in the reference list of this paper. Reference 22 should have been:

Sharpeshkar, R. Analog versus digital: extrapolating from electronics to neurobiology. *Neural Comput.* **10,** 1601–1638 (1998).

Also, the following reference was omitted but should have been cited along with refs 5–9 at the top of page 948.

Douglas R. J., Koch, C., Mahowald, M. A., Martin, K. A. C. & Suarez, H. Recurrent excitation in neocortical circuits. *Science* **269,** 981–985 (1995). □